

# Semianalytical Models of Sprite Formation from Plasma Inhomogeneities

V. V. Surkov<sup>a, b, \*</sup> and M. Hayakawa<sup>c</sup>

<sup>a</sup>National Research Nuclear University MEPhI, Moscow, 115409 Russia

<sup>b</sup>Pushkov Institute of Terrestrial Magnetism, Ionosphere, and Radiowave Propagation,  
Russian Academy of Sciences (IZMIRAN), Troitsk, Moscow, 142190 Russia

<sup>c</sup>Telecommunication University, Tokyo, Japan

\*e-mail: surkovvadim@yandex.ru

Received September 17, 2015; in final form, February 1, 2016

**Abstract**—A spherical plasma inhomogeneity located at mesospheric altitudes in a thundercloud quasi-electrostatic field is considered as a possible cause of sprite formation. A simple semianalytical model of ionization instability in a quasi-electrostatic field, the value of which is larger than the air breakdown value, is developed on the assumption that plasma ball conductivity is controlled by impact ionization and electron attachment to neutrals. After several simplifications, the problem is reduced to a system of ordinary differential equations for the average conductivity and plasma ball radius. The analytical estimates and numerical simulation indicate that the predicted expansion rate and acceleration of the plasma inhomogeneity boundary are close in magnitude to the values observed during high-speed imaging of sprite development.

DOI: 10.1134/S0016793216050145

## 1. INTRODUCTION

The data from high-speed imaging indicated that sprites can be initiated spontaneously at mesospheric altitudes or can originate from the luminous inhomogeneities that appear at the halo bottom. Sprite-initiating streamers, which start developing downward and upward from a sprite initiation point, appear subsequently (Cummer et al., 2006). Based on high-speed imaging methods with a time resolution of 1 ms, Stanley et al. (1999) established that the growth rates of initial streamers are higher than  $10^7$  m/s. Multinode photometer observations indicated that the velocities of downward and upward propagating streamers are about  $10^7$ – $10^8$  m/s (McHarg et al., 2002). An analysis of the data on high-speed imaging with a time resolution of 0.1 ms made it possible to establish that streamers develop with an acceleration about  $10^{10}$  m s<sup>-2</sup> at a sprite top during the initial stage of development (McHarg et al., 2007). At the same time, at the sprite bottom, downward-propagating streamers first accelerate to the maximal velocity  $(1–3) \times 10^7$  m/s and then abruptly decelerate with an almost constant rate close to  $10^{10}$  m s<sup>-2</sup>, and this deceleration dominates in the course of time and over a distance traveled by these streamers (Li and Cummer, 2009).

The numerical simulation of a streamer sprite development in the external electric field, which is close to the conventional breakdown threshold, indi-

cates that a streamer can propagate with an acceleration about  $(0.5–1) \times 10^{10}$  m s<sup>-2</sup> during the initial stage (Liu et al., 2009; Kosar et al., 2012). In another numerical model, a downward-propagating streamer is formed at the front of an electron density wave, which in turn originates from the sprite halo after a positive cloud-to-ground lightning discharge (Luque and Ebert, 2009, 2010). Pasko et al. (2013) indicated that the numerical calculations performed in (Luque and Ebert, 2009, 2010) cannot explain the experimentally observed initial acceleration of streamers. In addition, it was assumed that a collapse of the electron density wave front, which transforms this front into a streamer, can be caused by the instability of the finite-difference schemes that were used to numerically simulate the equations (Qin et al., 2011). The model of a sprite in the form of an expanding ball filled with electron avalanches was considered in (Qin et al., 2011). It was assumed that this ball expands due to both the electrostatic repulsion and diffusion of produced electron avalanches. A more detailed review of the theoretical and numerical studies of the sprite evolution can be found in (Raizer et al., 2010; Evtushenko and Mareev, 2011; Surkov and Hayakawa, 2012; Pasko et al., 2013).

We note that the basic equations that describe the mesospheric electromagnetic field and the charged particle dynamics, including the processes of ionization and electron attachment and detachment from neutral air molecules as well as other reactions, are

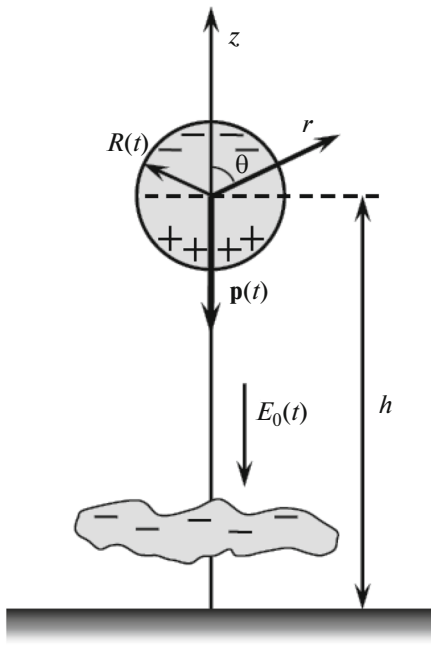


**Fig. 1.** Model of a plasma inhomogeneity located at altitude  $h$ . Downward arrow marks quasi-static field  $E_0(t)$  of thundercloud negative charges, and  $\mathbf{p}(t)$  is the plasma ball electric dipole moment.

complex. Mathematical analysis of these equations is often troublesome since there are many important parameters which approximately exponentially depend on altitude. Despite the considerable advances in studying this problem, numerical sprite simulation predominates over analytical studies.

This work is mainly aimed at developing simple models for the initial phase of sprite formation and at estimating analytically the expansion velocity and acceleration of the boundary of the region where streamers sprite development are generated.

## 2. THE SIMPLEST MODEL OF SPRITE INITIATION

Numerous measurements indicated that sprites are mostly generated by intense lightning discharges with a charge moment higher than 500 C km, which transfers positive charge to the ground (Boccippio et al., 1995). After such a lightning discharge, an uncompensated negative electric charge appears in a thundercloud for a short time, which in turn results in the formation of a transient electric field in the atmosphere. Following (Qin et al., 2011), we assume that a sprite starts developing from a spherical conducting plasma inhomogeneity located above a thundercloud at altitudes of 60–80 km. If electric field of the cloud charges is higher than the conventional breakdown threshold,  $E_c$ , at these altitudes, this will result in addi-

tional plasma production within an inhomogeneity, as a result of which the radius ( $R$ ) of this inhomogeneity will start increasing.

The onset of a primary streamer growth within an inhomogeneity can be initiated by an individual electron avalanche, which starts at any local plasma density fluctuation or, for example, at a claw on the plasma inhomogeneity surface, where polarization charges accumulate that results in a local electric field enhancement up to a value which is larger than  $E_c$  by several times. A close analogy exists with point-to-plane corona discharges as observed during laboratory tests (Raizer, 2009). Note that a formed streamer can propagate into the regions where the electric field is lower than the conventional breakdown threshold.

The considered model is schematically shown in Fig. 1. Here  $E_0$  is the strength of the electric field of thundercloud negative charges and charges induced in a conducting ground. Since the altitude ( $h$ ) where the inhomogeneity center is located is much larger than the inhomogeneity radius ( $R$ ), we can consider that field  $E_0$  in the vicinity of an inhomogeneity is almost homogeneous. We will consider this field as a given slowly varying function of time  $E_0 = E_0(t)$ . We first consider the simplest model of inhomogeneity, in which the plasma conductivity ( $\sigma$ ) is considered constant. In the next section, we will generalize this model by incorporating the dependence of the plasma conductivity on the rates of ionization and electron attachment to neutrals, which are in turn the functions of an external electric field. Ambient air conductivity  $\sigma_0$  in the vicinity of a ball is also considered constant. The assumption that the inhomogeneity spherical shape is unchanged decreases the application field of this model; on the other hand, such an approach will make it possible to give an analytical estimate of the plasma inhomogeneity expansion rate and to compare this value with the actual sprite formation rate.

A quasi-stationary electric field ( $\mathbf{E}$ ) of cloud and plasma ball charges satisfies the Maxwell equation  $\nabla \times \mathbf{E} = 0$  and can therefore be expressed in terms of potential  $\varphi$  in a usual fashion; i.e.,  $\mathbf{E} = -\nabla\varphi$ . Taking also into account the continuity equation  $\nabla \cdot \mathbf{j} = 0$ , where  $\mathbf{j} = \sigma\mathbf{E} + \varepsilon_0 \partial\mathbf{E}/\partial t$  is the total current density and  $\varepsilon_0$  is the electric constant, we arrive at the Laplace equation for potential:  $\nabla^2\varphi = 0$ . This equation is valid not only for a plasma ball but also for the environment. The sense of this equation is that the electric charge density is zero in this approximation everywhere except the inhomogeneity surface, where the discontinuity in the medium conductivity occurs.

We place the origin of the spherical coordinate system at the ball center, having directed the  $z$  axis vertically upward, i.e., opposite to the direction of field  $\mathbf{E}_0$ . The boundary conditions for the Laplace equation are

the continuity of the potential and current density normal component on the ball surface at  $r = R$ :

$$\varphi_1 = \varphi_2, \quad \sigma E_{1r} + \varepsilon_0 \frac{\partial E_{1r}}{\partial t} = \sigma_0 E_{2r} + \varepsilon_0 \frac{\partial E_{2r}}{\partial t}. \quad (1)$$

In the  $r > R$  region, we search the solution of the Laplace equation in the form  $\varphi_2 = \varphi_0 + \varphi'_2$ , where  $\varphi_0$  is the thundercloud charge potential, and  $\varphi'_2$  describes disturbances caused by electric charges induced on the ball surface. Taking into account that a disturbed field belongs to the dipole type, we obtain (Landau and Lifshits, 1982):

$$\varphi_2 = E_0 r \cos \theta - \frac{kp \cos \theta}{r^2}, \quad (2)$$

where  $\theta$  is the polar angle shown in Fig. 1;  $k = (4\pi\varepsilon_0)^{-1}$ ;  $\varepsilon_0$  is the electric constant;  $p = p(t)$  is the ball effective dipole moment.

In the  $r < R$  region, we find the solution in the form of homogeneous field  $\mathbf{E}_1(t)$  with potential

$$\varphi_1 = E_1 r \cos \theta. \quad (3)$$

Substituting relationships (2) and (3) for potentials  $\varphi_1$  and  $\varphi_2$  in boundary conditions (1), we obtain

$$E_0 - \frac{kp}{R^3} = E_1, \quad (4)$$

$$\frac{dE_1}{dt} + \frac{E_1}{T} = \frac{dE_0}{dt} + \frac{E_0}{T_0} + \frac{2k}{R^3} \left( \frac{dp}{dt} + \frac{p}{T_0} \right), \quad (5)$$

where  $T = \varepsilon_0/\sigma$  and  $T_0 = \varepsilon_0/\sigma_0$  are the relaxation times related to the ball and ambient air conductivities. If the  $E_0(t)$  function is specified, we can find unknown functions  $E_1(t)$  and  $p(t)$  from Eqs. (4) and (5). Note that these equations are reduced to the electrostatic problem at constant  $E_0$  and  $\sigma_0 = 0$ , the solution to which is known (Landau and Lifshits, 1982).

The conventional breakdown threshold depends on altitude:  $E_c = E_* \exp(-z/l)$ , where  $l = 8-10$  km, and  $E_*$  is the breakdown threshold value at an air pressure at sea level ( $z = 0$ ) (see, e.g., (Surkov and Hayakawa, 2012)). If the electric field in the vicinity of a ball is on average larger than the threshold value  $E_c$ , the air ionization and the electron avalanche formation result in the appearance of free electrons and ions, thereby increasing the plasma ball dimension. Therefore, we assume that the electric field at the ball bottom is greater than or equal to the threshold value at this altitude; i.e.,  $E = nE_c$ , where  $n \geq 1$  is a certain constant. From this it follows that

$$E_0 + \frac{2kp}{R^3} = nE_* \exp\left(\frac{R-h}{l}\right). \quad (6)$$

For higher altitudes, condition  $E > nE_c$ , will be satisfied since the electric field of thundercloud

charges and charges induced in a conducting ground decreases with altitude as  $z^{-3}$ , i.e., slower than field  $E_c$ .

Solving Eqs. (4)–(6) for  $R(t)$ , we obtain:

$$\begin{aligned} & \frac{dR}{dt} \left[ \left( 2 + \frac{R}{l} \right) nE_* \exp\left(\frac{R-h}{l}\right) - 2E_0 \right] \\ & = R \left[ \frac{E_0}{T} + \frac{dE_0}{dT} - \left( \frac{2}{T_0} + \frac{1}{T} \right) \frac{nE_*}{3} \exp\left(\frac{R-h}{l}\right) \right]. \end{aligned} \quad (7)$$

Considering the increasing field  $E_0(t)$ , we noted that Eqs. (6) and (7) are both valid beginning with the moment  $t = t_*$  when the field  $E_0$  reaches the threshold value  $nE_c$ ; that is, under requirement that  $E_0(t_*) = nE_c(h) = nE_* \exp(-h/l)$ . To simplify the problem, we neglect the initial dimension of a plasma inhomogeneity, assuming that  $R(t_*) = 0$  at that instant and, consequently,  $p(t_*) = 0$ . For convenience, we also introduce the following dimensionless variables and functions:

$$\tau = \frac{t - t_*}{T_0}, \quad u(\tau) = \frac{R(\tau)}{l}, \quad f(\tau) = \frac{E_0(\tau)}{nE_c(h)}, \quad (8)$$

where  $f(0) = 1$ , and  $u(0) = 0$ .

Since the inhomogeneity dimension is assumed to be small; i.e.,  $R \ll l$ , then  $u \ll 1$  and, consequently,  $\exp(u) \approx 1 + u$ . In addition, during a short period after  $t = t_*$ , function  $f$  can be approximated as follows:  $f = 1 + \dot{f}(0)\tau$ , where a dot above symbol  $f$  denotes a derivative with respect to  $\tau$ . In such a case, Eq. (7) is simplified to the form:

$$\frac{du}{d\tau} = \frac{us}{3u - 2\dot{f}(0)\tau}, \quad (9)$$

where  $s = 2(\sigma/\sigma_0 - 1)/3 + \dot{f}(0)$ . The general solution of Eq. (9) has the form:

$$u^{2\dot{f}(0)} \left| u - \frac{\tau}{3} [2\dot{f}(0) + s] \right|^s = C, \quad (10)$$

where  $C$  is an arbitrary constant. In particular, the solution passing through point  $(0,0)$ , has the form:  $u = \tau\{\dot{f}(0) + (2/9)(\sigma/\sigma_0 - 1)\}$ . Returning to the dimensional variables, we obtain dependence  $R = V\Delta t$ , where  $\Delta t = t - t_*$ , and

$$V = \dot{R} = \frac{1}{T_0} \left\{ \frac{T_0 \dot{E}_0(t_*)}{nE_c(h)} + \frac{2}{9} \left( \frac{\sigma}{\sigma_0} - 1 \right) \right\}. \quad (11)$$

Here a dot above symbol  $E_0$  denotes the time derivative taken at  $t = t_*$ .

The quasi-static electric field ( $E_0$ ) of cloud charges and their electric images in the ground can be described by the effective electric dipole field with moment  $D(t)$ , which depends on the charge distribution in a cloud. We use the following approximation as an example:

$$D = D_m \frac{t}{t_r} \exp\left(-\frac{t}{t_r}\right), \quad (12)$$

where  $D_m$  is the dipole moment maximal value and  $t_r$  is the charge relaxation characteristic time. Taking into account that  $E_0$  is proportional to dipole moment  $D(t)$ , we find that  $\dot{E}_0(t_*) = nE_c(h) \times (t_*^{-1} - t_r^{-1})$ . To estimate the ball expansion rate ( $V$ ), we use the following parameter values:  $l = 8$  km,  $t_r = 10$  ms, and  $t_* = 2$  ms. The atmospheric air conductivity at an altitude of 70 km varies from  $10^{-9}$  S m $^{-1}$  (nighttime conditions) to  $5 \times 10^{-7}$  S m $^{-1}$  (daytime conditions) depending on solar activity (see, e.g., (Surkov and Hayakawa, 2014)). The plasma conductivity ( $\sigma$ ) at mesospheric altitudes mostly depends on the electron density since the electron mobility is much greater than the ion mobility. Numerical simulation of the sprite evolution (Pasco et al., 2013) indicated that electrons are nonuniformly distributed in sprite space. In this case their density is maximal near streamer heads. In the scope of the model alluded to above, conductivity  $\sigma$  can be considered only as a quantity averaged over the plasma ball volume. Substituting the  $\sigma_0 = 10^{-8}$  S m $^{-1}$  and  $\sigma = (3 - 30)\sigma_0$  values and the above parameters in (12), we roughly estimate that  $V \approx (7 - 61) \times 10^6$  m/s.

This estimate is close in an order of magnitude to the observed velocity of streamers that form a sprite under nighttime conditions. However, the constancy of velocity  $V$  in formula (11) means that this simplified model cannot be applied to individual streamers even qualitatively, since the experimental streamer velocity is variable (Li and Cummer, 2009). In the next section, we extend this model by incorporating the processes of ionization and electron attachment to air molecules.

### 3. EFFECTS OF IONIZATION AND ELECTRON ATTACHMENT TO MOLECULES

Plasma conductivity variations at mesospheric altitudes are described by the following approximate equation (Luque and Ebert, 2009):

$$\frac{\partial \sigma}{\partial t} = \mu(\nabla \cdot \mathbf{j}_c) + (v_i - v_a)\sigma + e\mu S_{ph}, \quad (13)$$

where  $\mu$  is the electron mobility;  $\mathbf{j}_c$  is the density of the electric current resulted from plasma conductivity and electron diffusion;  $v_i$  and  $v_a$  are the rates of impact ionization and electron dissociative attachment, respectively; and  $S_{ph}$  is a nonlocal photoionization source. The ion current and conductivity are ignored in this approximation, since it is assumed that the ion mobility can be neglected as compared to the electron mobility. The reaction rate difference  $v_i - v_a$  can be approximated as follows:

$$v_i - v_a = \mu_* E \left\{ \alpha_{i0} \exp\left(-\frac{E_i}{E}\right) - \alpha_{a0} \exp\left(-\frac{E_a}{E}\right) \right\}. \quad (14)$$

Here  $\mu_* \approx 3.8 \times 10^{-2}$  m $^2$  V $^{-1}$  s $^{-1}$  is the electron mobility at an air pressure at sea level;  $\alpha_{i0} \approx 4.3 \times 10^5$  m $^{-1}$  and  $\alpha_{a0} \approx 2 \times 10^3$  m $^{-1}$  are the empirical constants. Critical fields  $E_i$  and  $E_a$ , responsible for the ionization and electron attachment rates, exponentially depend on altitude; i.e.,  $E_i = E_{i0} \exp(-z/l)$ , and  $E_a = E_{a0} \exp(-z/l)$ , where  $E_{i0} = 2 \times 10^7$  V m $^{-1}$ , and  $E_{a0} = 3 \times 10^6$  V m $^{-1}$  (Luque and Ebert, 2009). Note that the conventional air breakdown threshold ( $E_c$ ) satisfies condition  $v_i = v_a$ .

Following (Hu et al., 2007; Hiraki and Fukunishi, 2006), we leave only one term in the right-hand side of Eq. (13):  $(v_i - v_a)\sigma$ , assuming that this term is much greater than the remaining terms. In this approximation the plasma conductivity within a ball is homogeneous and Eq. (13) will describe the time dependence of the average plasma conductivity. In the scope of a given model, this agrees with the fact that the electric field within a ball ( $E_1$ ) is assumed to be homogeneous and dependent only on time.

Introducing a new dimensionless function  $w(\tau) = \sigma(\tau)/\sigma_0 - 1$ , substituting dimensionless functions  $w(\tau)$ ,  $u(\tau)$  and variable  $\tau$  in Eqs. (7) and (13), we arrive at the following equation set:

$$\begin{aligned} & \frac{du}{d\tau} [(2+u)\exp(u) - 2f] \\ & = u \left[ (1+w)f + \frac{df}{d\tau} - \left(1 + \frac{w}{3}\right)\exp(u) \right], \end{aligned} \quad (15)$$

$$\begin{aligned} \frac{dw}{d\tau} & = \mu_* E_1 T_0 \left[ \alpha_{i0} \exp\left(-\frac{E_i}{E_1}\right) \right. \\ & \left. - \alpha_{a0} \exp\left(-\frac{E_a}{E_1}\right) \right] (1+w), \end{aligned} \quad (16)$$

where functions  $E_i$  and  $E_a$  are taken at  $z = h$ , and  $f(\tau)$  is the specified dimensionless function that describes the evolution of a quasi-stationary field of cloud charges and their electric images in a conducting ground. Recall that this field is larger than the air-breakdown threshold ( $nE_c$ ) at altitude  $z = h$ , beginning from instant  $\tau = 0$ , when  $f(0) = 1$ . The following analysis will indicate that the plasma ball conductivity strongly increases with time; therefore, the difference in the initial conductivities of a ball and ambient air is not so substantial. We will subsequently neglect this difference as well as the initial ball radius. Thus, the initial problem conditions are as follows:  $u(0) = w(0) = 0$ .

We will first find the approximate solution of Eqs. (15) and (16) for the initial ball development stage. The ball electric field is initially close to  $nE_c(h)$ , and the expression in square brackets in Eq. (16) can therefore

be expanded into a series in terms of small parameter  $E_1 - nE_c(h)$ . Transforming relationships (4) and (6), we find that  $E_1 = nE_c \times (h) \{3f(\tau) - \exp(u)\}/2$ . After these simplifications, Eq. (16) is reduced to the form:

$$\frac{dw}{d\tau} = \left\{ A + \frac{B}{2} [3f - 2 - \exp(u)] \right\} (1 + w). \quad (17)$$

We used here the following abbreviations:

$$A = \mu_* n E_c(h) T_0 (s_i - s_a), \quad (18)$$

$$B = \mu_* n E_c(h) T_0 \left[ s_i \left( 1 + \frac{E_{i0}}{nE_*} \right) - s_a \left( 1 + \frac{E_{a0}}{nE_*} \right) \right], \quad (19)$$

where

$$s_{i,a} = \alpha_{i0,a0} \exp\left(-\frac{E_{i0,a0}}{nE_*}\right). \quad (20)$$

As before, we first assume that variable  $\tau$  and functions  $u$  and  $w$  are much less than unity. In this case we find the solutions of the equations in the form of the series

$$u = \sum_{k=1}^{\infty} c_k \tau^k, \quad w = \sum_{k=1}^{\infty} b_k \tau^k. \quad (21)$$

Expanding  $\exp(u)$  into a series as powers of  $u$  and substituting series (21) in Eqs. (15) and (17), we arrive at the recurrent relationships for unknown coefficients  $c_k$  and  $b_k$ . Finding these coefficients, we finally obtain:

$$\begin{aligned} u &= \dot{f}\tau + \left( \ddot{f} - \dot{f}^2 + \frac{A}{3} \right) \frac{\tau^2}{2} \\ &+ \left( \frac{B\dot{f}}{15} + \frac{\ddot{f} + 2\dot{f}^3 - 3\dot{f}\ddot{f}}{6} \right) \tau^3 + \dots, \\ &+ \frac{A}{30} \left[ 2A + 2\dot{f} - \frac{3\ddot{f} + A}{\dot{f}} - 1 \right] \tau^3 + \dots, \\ w &= A\tau + \frac{(B\dot{f} + A^2)}{2} \tau^2 \\ &+ \left\{ \frac{B}{2} \left( \ddot{f} - \frac{A}{6} + 3\dot{f}A \right) + \frac{A^3}{3} \right\} \frac{\tau^3}{3} + \dots, \end{aligned} \quad (22)$$

where the derivatives of  $f$  are taken at  $\tau = 0$ .

We first consider a simple case when  $n = 1$ . In such a case,  $s_i = s_a$ ,  $A = 0$ , and the expression for  $B$  is reduced to the form  $B = GT_0 E_c(h)$ , where

$$G = \mu_* \alpha_{i0} \left( \ln \frac{\alpha_{i0}}{\alpha_{a0}} \right) \left( \frac{\alpha_{a0}}{\alpha_{i0}} \right)^{E_{i0}/(E_{i0} - E_{a0})}. \quad (24)$$

Using  $E_* = 32 \text{ kV cm}^{-1}$ ,  $h = 70 \text{ km}$ , and the above parameters, we find that  $E_c(h) = 0.51 \text{ kV m}^{-1}$  and  $G \approx 1.6 \times 10^2 \text{ m V}^{-1} \text{ s}^{-1}$ .

Having taken the time derivative of expression (22), we find the plasma ball expansion rate. In dimensional variables we obtain:

$$\begin{aligned} V &= \frac{l\dot{E}_0}{E_c(h)} \left[ 1 + \left( \frac{\ddot{E}_0}{\dot{E}_0} - \frac{\dot{E}_0}{E_c(h)} \right) \Delta t \right. \\ &\quad \left. + \frac{GE_c(h)}{5T_0} \Delta t^2 + \dots \right], \end{aligned} \quad (25)$$

$$\sigma = \sigma_0 \left( 1 + G\dot{E}_0 \Delta t^2 + \frac{G\ddot{E}_0}{3} \Delta t^3 + \dots \right), \quad (26)$$

where dots above symbol  $E_0$  mean time derivatives taken at instant  $t = t_*$ . Using a dipole moment approximation in form (12), we obtain

$$\dot{E}_0 = E_c(h) \left( \frac{1}{t_*} - \frac{1}{t_r} \right), \quad \ddot{E}_0 = -\frac{E_c(h)}{t_r} \left( \frac{2}{t_*} - \frac{1}{t_r} \right). \quad (27)$$

High-speed imaging indicates (Stanley et al., 1999; McHarg et al., 2002; Cummer et al., 2006) that the sprite development characteristic time is 1–3 ms. For example, substituting  $\Delta t = 2 \text{ ms}$  and the above parameters in relationships (25) and (26), we obtain the following rough estimates:  $V = 1.5 \times 10^7 \text{ m/s}^2$ ,  $\dot{V} = 1.5 \times 10^{10} \text{ m/s}$ , and  $\sigma = 5.6\sigma_0$ . Note that the last term in relationship (25) is much less than the remaining terms if  $\Delta t > 0.5 \text{ ms}$ . In this case relationship (25) is simplified to the form:

$$V \approx \frac{lG\dot{E}_0(t_*)}{5T_0} \Delta t^2. \quad (28)$$

Comparing expressions (11) and (25), we can note that the nonlinear dependence of the expansion rate on time (25) is obtained in a more detailed model as compared to the simplest model considered in Section 2. In addition, since solutions (22) and (23) contain factor  $B$ , which depends on the parameters of the impact ionization and electron dissociative attachment; this results in a numerical estimate of the expansion rate (25) that is higher than that in the simplest model.

The plasma electron density can be estimated as  $n_e = \sigma/(e\mu)$ , where  $\mu = \mu_* \exp(h/l)$  is the electron mobility at altitude  $h$ . Substituting the above parameters into these relationships, we obtain  $n_e = 1.5 \times 10^9 \text{ m}^{-3}$ . The results of the numerical simulation (Pasko et al., 2013) indicate that the electron density in a sprite streamer head can be approximately two orders of magnitude as high as the density obtained by us. We will discuss this discrepancy later.

The analytical estimates obtained above can be applied during the initial stage of the plasma inhomogeneity development. To trace the inhomogeneity further evolution, we next perform the numerical integration of Eqs. (15) and (16). As before, we assume that the breakdown threshold  $E_0(t)$  is higher than the air breakdown field strength at altitude  $z = h$ , beginning from instant  $t = t_*$ . The  $\tau$ -dependence of electric

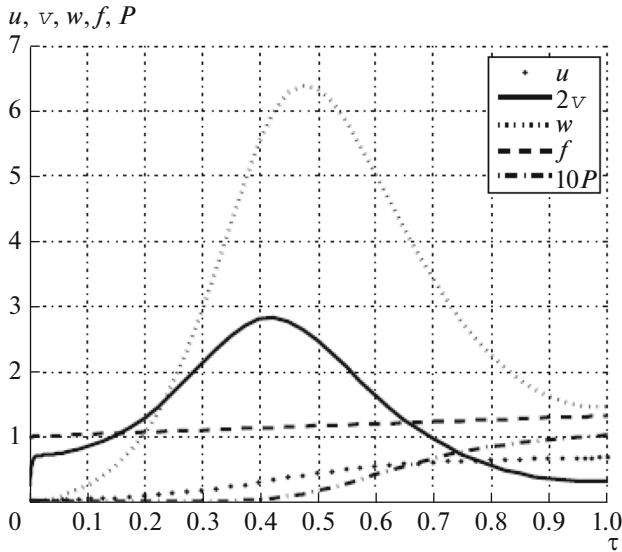


**Fig. 2.** Dimensionless radius  $u$  and expansion rate  $v$ , a change in the conductivity ( $w$ ), the plasma ball electric moment ( $P$ ), and the cloud charge electric field ( $f$ ) depending on dimensionless time  $\tau$ . For convenience, the  $v$  and  $P$  plots are multiplied by 2 and 10, respectively.

dipole moment (12) of cloud charges and charges induced in the ground is given by:

$$f(\tau) = \left(1 + \frac{\tau T_0}{t_*}\right) \exp\left(-\frac{\tau T_0}{t_r}\right). \quad (29)$$

Note that Eq. (15) has a singularity at initial integration point  $(\tau, u, w) = (0, 0, 0)$ , since both sides of this equation vanish at this point. Therefore, we first use analytical solution (22), (23), which specifies the integral curve passing through the singular point, and then perform a numerical integration of these differential equations. Figure 2 illustrates the calculations of plasma ball dimensionless radius  $u = R/l$ , expansion rate  $v = du/d\tau$ , and conductivity  $w = \sigma/\sigma_0 - 1$ , as well as the ball dimensionless dipole moment  $P(\tau) = kp(\tau)/[l^3 E_c(h)]$  and function  $f(\tau)$ , which is proportional to cloud charge dipole moment  $D(\tau)$  versus dimensionless time  $\tau = (t - t_*)/T_0$ . For convenience, we multiplied the  $v$  and  $P$  plots by 2 and 10, respectively. In the calculations we used the parameter values indicated above.

The plots indicate that the expansion rate ( $v$ ) and plasma conductivity ( $w$ ) reach maximal values in the interval  $\tau = 0.4-0.5$ . In dimensional variables the maximal velocity and conductivity values are  $V = 1.3 \times 10^7$  m/s and  $\sigma = 7.4 \times 10^{-8}$  S m<sup>-1</sup>. These values subsequently decrease and are accompanied by almost synchronous damping oscillations with period  $\tau \sim 1$ .

These oscillations are not shown in Fig. 2, since they have not physical meaning at first glance and cannot be implemented in practice. Nevertheless, we will discuss later the cause and possible physical sense of a nonmonotonic behavior of  $v$  and  $w$  originating in this model.

#### 4. MODEL GENERALIZATION FOR THE FIELD EXCEEDING THE AIR ELECTRIC BREAKDOWN THRESHOLD

As was mentioned above, parameter  $\sigma$ , which acts as a conductivity averaged over the inhomogeneity volume, should be smaller than the plasma conductivity at a streamer head. The spherical geometry of the problem and the assumption that  $n = 1$ , which means that  $E = E_c$  at the plasma ball bottom, are important factors affecting the  $\sigma$  value in the scope of this model. We now extend the model applicability region, assuming that the electric field at the ball bottom is  $nE_c$ , i.e., is larger than the air breakdown threshold at a given altitude by constant factor  $n > 1$ . We first find an approximate solution of Eqs. (15) and (17) at  $\tau \ll 1$  in the form of power series (21). In a first approximation, we obtain

$$w = A\tau, \quad u = \dot{f}\tau + \left(\ddot{f} - \dot{f}^2 + \frac{A}{3}\right) \frac{\tau^2}{2}. \quad (30)$$

The term of the second order of smallness is kept in the expression for  $u$ , because parameter  $A$  is large as compared to  $\dot{f}$ . Therefore, the approximate formula for the dimensional expansion rate has the form

$$V \approx \left( \frac{\dot{E}_0}{nE_c(h)} - \frac{\dot{E}_0^2}{n^2 E_c^2(h)} + \frac{A}{3T_0^2} \right) l \Delta t. \quad (31)$$

Consequently, the expansion rate and a change in the plasma conductivity  $\Delta\sigma = \sigma_0 w$  increase approximately linearly in the course of time at least during the initial development stage. The  $V$  value in relationship (31) is affected by two factors: the rate of a change in quasi-stationary field  $E_0$  and its derivative as well as the ionization and electron attachment rates that are described by term  $A/(3T_0^2)$ . If the first two terms in the right-hand side of expression (31) prevail, rate  $V$  mainly depends on time derivatives of  $E_0$ . In this case these two terms act as an external ionizer by analogy with a nonself-sustained gas discharge. However, the numerical estimates indicate that term  $A/(3T_0^2)$  in expression (31) is maximal. Therefore, the ionization and electron attachment parameters are important factors affecting the development of a plasma inhomogeneity.

Taking  $n = 1.2$  and substituting the parameters used above in relationship (31), we find that the rate is  $V \approx 3.5 \times 10^7$  m/s at  $\Delta t = 2$  ms. This value is larger

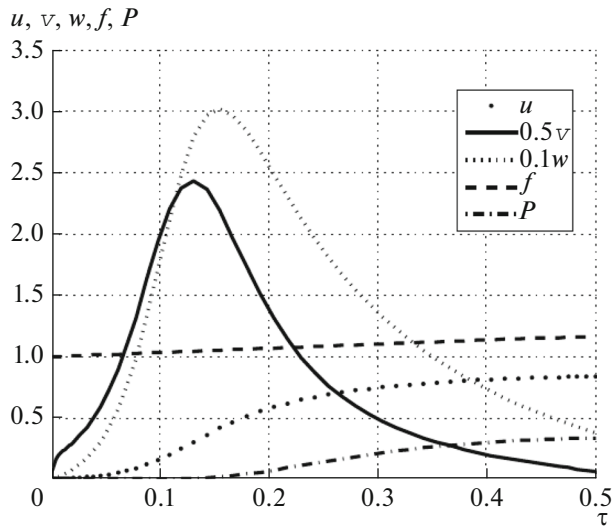


**Fig. 3.** The same dependences that are presented in Fig. 2 but for  $n = 1.2$ . For convenience, the  $w$  and  $v$  plots are multiplied by 0.1 and 0.5, respectively.

than the previous  $V$  value for the same instant. Figure 3 illustrates results of the numerical integration of Eqs. (15) and (16) at the same parameters. A comparison of Figs. 2 and 3 indicates that an insignificant increase in factor  $n$  results in a considerable increase in the expansion rate and plasma ball conductivity. We can analyze the dependence of  $V$  on the growth rate of the cloud electric field by varying parameter  $t_*$  in relationship (27). Figure 4 shows the time variations in the plasma ball expansion rate at  $t_* = 2, 5, 9$  ms.

The numerical simulation (Pasko et al., 2013) of the sprite development indicated that the electron

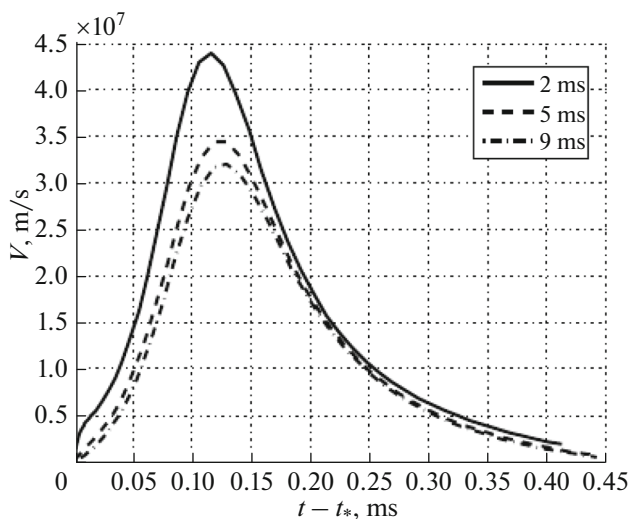


**Fig. 4.** Plasma ball expansion rate depending on time at  $t_* = 2, 5,$  and  $9$  ms.

density at a streamer head can be higher than  $10^{12} \text{ m}^{-3}$  at an altitude of 70 km at  $n = 1.5$ . To demonstrate that the electric field is larger than the air breakdown threshold,  $n$ -dependences of dimensionless peak velocity  $v_{\text{max}} = (du/d\tau)_{\text{max}}$  and plasma conductivity  $w_{\text{max}}$  are shown in Fig. 5. An analysis of these dependences indicates that an approximately linear relation exists between these parameters:  $w_{\text{max}} \approx 8(v_{\text{max}} - 1)$ . An increase in the plasma conductivity to  $\sim 100\sigma_0$  at  $n = 1.4$  results in an increase in the plasma density to  $n_e = 3 \times 10^{11} \text{ m}^{-3}$ , which is close to the average electron density calculated for streamers using the numerical simulation (Pasko et al., 2013). Nevertheless, in the scope of this model, it is impossible to take into account an actual streamer head curvature and to estimate the local electron density at tops of sprite streamers. Moreover, the application field of the spherically symmetric model is restricted by the values of  $n$  below 1.2–1.3 because the velocity  $V_{\text{max}} = v_{\text{max}}I/T_0$  shown in Fig. 5 at  $n > 1.2$ –1.3 is too high to be in agreement with the observations.

## 5. DISCUSSION

The performed calculations indicated that the rate of the plasma inhomogeneity boundary expansion ( $V$ ) coincides with the sprite streamer velocity in an order of magnitude. It is interesting to note that the model, which takes into account the impact ionization and dissociative attachment of electrons to air molecules, results in nonlinear dependence  $V(t)$ , which generally agrees with the observations of streamers moving downward from a sprite initiation point (Li and Cummer, 2009). On the calculated and experimental plots, the velocity first increases, reaching its maximal value

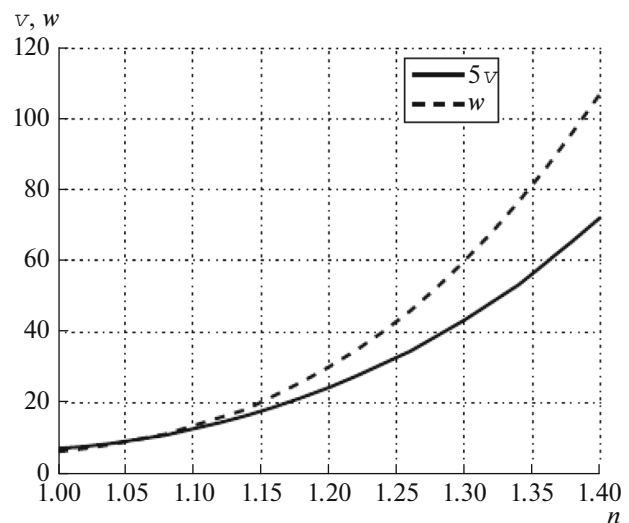


**Fig. 5.** Dimensionless maximal expansion rate and conductivity as functions of  $n$ .

(about  $10^7$  m/s) at  $t \approx 0.2\text{--}0.3$  ms, and subsequently starts decreasing. In some experiments it was found that the velocity of sprite-initiating streamers demonstrates insignificant damping oscillations with a period of  $0.2\text{--}0.4$  ms as they propagate downward (see, e.g., Fig. 1 in (Li and Cummer, 2009)). Note that the numerical solution of Eqs. (15) and (16) exhibits the similar oscillations in the inhomogeneity expansion rate in the region of dimensionless time  $\tau \sim 1$ .

Taking this similarity into account, we discuss the possible cause of such a phenomenon, even though the our model does not describe individual streamers and, generally speaking, can be applied at small  $\tau$  values.

Outside a plasma ball near its bottom and top points,  $z = h \mp R$ , the electric field strength is  $E_2 = E_0 + 2kp/R^3$ , i.e., is larger than the external electric field  $E_0$ . Within a ball, the field is constant and is  $E_1 = E_0 - kp/R^3$ , i.e., is smaller than  $E_0$ , owing to the screening effect of charges induced on the ball surface. According to the following equation:  $\partial\sigma/\partial t = (v_i - v_a)\sigma$  and relationship (14), both the difference in the rates of ionization and electron attachment and the plasma conductivity within a ball, depend on the internal field  $E_1$ . An analysis of Eqs. (15) and (16) indicates that  $E_1$  is first greater than the critical breakdown field  $E_c(h)$  at a given altitude ( $h$ ); i.e., the air ionization within a plasma ball predominates since  $v_i > v_a$ . The dipole moment  $p$  of induced charges increases in this case, which can result in a decrease in  $E_1$  to values smaller than  $E_c(h)$ , whereas  $E_2 > E_c(h)$  outside a ball as before. This means that  $v_i < v_a$ ; i.e., the electron attachment to molecules prevails during some periods and will be accompanied by a decrease in the conductivity and ball expansion rate. In an increasing external electric field ( $E_0$ ), these two opposite tendencies can alternate and cause sign reversal  $\partial\sigma/\partial t$ . The observations of the streamer head luminescence variations, which can be resulted from the weak oscillations in the plasma conductivity and the Lenz–Joule heating rate in the streamer heads might serve as indirect evidence in support of and against this hypothetical possibility.

## 6. CONCLUSIONS

The foregoing study indicated that an increasing thundercloud charge field during the continuing current stage at the end of a lightning discharge can initiate an increase in the plasma inhomogeneity at mesospheric altitudes if the cloud field strength is higher than the air breakdown threshold ( $E_c$ ) at these altitudes. An analysis of the semianalytical plasma inhomogeneity model, in which the impact ionization and

electron dissociative attachment to air molecules were taken into account, indicated that the inhomogeneity boundary expansion rate and the inhomogeneity conductivity increase nonlinearly in the course of time.

The maximal rates of expansion  $V_{\max} \sim 10^7$  m/s and acceleration  $\sim 10^{10}$  m s<sup>-2</sup> are close to the experimentally observed values for sprite-initiating streamers. The plasma inhomogeneity conductivity calculated in the model is lower than the conductivity that was predicted by other researchers using the numerical simulation. However, if we assume that the electric field at the inhomogeneity bottom is larger than  $E_c$  and is equal to  $nE_c$ , where the constant factor is  $n = 1.1\text{--}1.4$ , then the maximal plasma conductivity ( $\sigma$ ) increases by one to two orders of magnitude and becomes close to the average  $\sigma$  value in streamers. Thus, all conditions for the origination of streamers are created within an inhomogeneity.

Our analytical estimates indicate that the inhomogeneity boundary expansion rate depends on the first and second time derivatives of the cloud charge electric field and on the parameters responsible for the rates of ionization and electron attachment to neutrals at mesospheric altitudes. In this case the latter factor, i.e., the ionization and electron attachment effect, makes apparently the maximal contribution, not only to the expansion rate but also to the plasma inhomogeneity conductivity. Therefore, the sprite initiation considered in this study can be interpreted as a certain form of the ionization instability of the mesospheric plasma inhomogeneity in an increasing quasi-static thundercloud charge field.

## ACKNOWLEDGMENTS

This work was supported by the Russian Foundation for Basic Research, project no. 13-05-12091. The work was partially supported by National Polar Research Institute, Tokyo.

## REFERENCES

- Boccippio, D.J., Williams, E.R., Heckman, S.J., Lyons, W.A., Baker, I.T., and Boldi, R., Sprites, ELF transients, and positive ground strokes, *Science*, 1995, vol. 269, no. 5227, pp. 1088–1091.
- Cummer, S.A., Jaugey, N., Li, J., Lyons, W.A., Nelson, T.E., and Gerken, E.A., Submillisecond imaging of sprite development and structure, *Geophys. Res. Lett.*, 2006, vol. 33, L04104. doi 10.1029/2005GL024969
- Evtushenko, A.A. and Mareev, E.A., Simulation of mesospheric-composition disturbances under the action of high-altitude discharges (sprites), *Radiophys. Quantum Electron.*, 2011, vol. 54, no. 2, pp. 111–127.
- Hiraki, Y. and Fukunishi, H., Theoretical criterion of charge moment change by lightning for initiation of sprites, *J. Geophys. Res.*, 2006, vol. 111, A11305. doi 10.1029/2006JA011729

- Hu, W., Cummer, S.A., and Lyons, W.A., Testing sprite initiation theory using lightning measurements and modeled electromagnetic fields, *J. Geophys. Res.*, 2007, vol. 112, D13115. doi 10.1029/2006JD007939
- Kosar, B.C., Liu, N., and Rassoul, H.K., Luminosity and propagation characteristics of sprite streamers initiated from small ionospheric disturbances at subbreakdown conditions, *J. Geophys. Res.*, 2012, vol. 117, A08328. doi 10.1029/2012JA017632
- Landau, L.D. and Lifshits, E.M., *Elektrodinamika sploshnykh sred* (Electrodynamics of Continuous Media), Moscow: Nauka, 1982.
- Li, J. and Cummer, S.A., Measurement of sprite streamer acceleration and deceleration, *Geophys. Res. Lett.*, 2009, vol. 36, L10812. doi 10.1029/2009GL037581
- Liu, N.Y., Pasko, V.P., Adams, K., Stenbaek-Nielsen, H.C., and McHarg, M.G., Comparison of acceleration, expansion, and brightness of sprite streamers obtained from modeling and high-speed video observations, *J. Geophys. Res.*, 2009, vol. 114, A00E03. doi 10.1029/2008JA013720
- Luque, A. and Ebert, U., Emergence of sprite streamers from screening-ionization waves in the lower ionosphere, *Nat. Geosci.*, 2009, vol. 2. doi 10.1038/ngeo662
- Luque, A. and Ebert, U., Sprites in varying air density: Charge conservation, glowing negative trails and changing velocity, *Geophys. Res. Lett.*, 2010, vol. 37, L06806. doi 10.1029/2009GL041982
- McHarg, M.G., Haaland, R.K., Moudry, D., and Stenbaek-Nielsen, H.C., Altitude–time development of sprites, *J. Geophys. Res.*, 2002, vol. 107, no. A11. doi 10.1029/2001JA000283
- McHarg, M.G., Stenbaek-Nielsen, H.C., and Kammer, T., Observations of streamer formation in sprites, *Geophys. Res. Lett.*, 2007, vol. 34, L08804. doi 10.1029/2006GL027854
- Pasko, V.P., Qin, J., and Celestin, S., Toward better understanding of sprite streamers: Initiation, morphology, and polarity asymmetry, *Surv. Geophys.*, 2013, vol. 34, no. 6, pp. 797–830. doi 10.1007/s10712-013-9246-y
- Qin, J., Celestin, S., and Pasko, V.P., On the inception of streamers from sprite halo events produced by lightning discharges with positive and negative polarity, *J. Geophys. Res.*, 2011, vol. 116, A06305. doi 10.1029/2010JA016366
- Raizer, Yu.P., *Fizika gazovogo razryada* (Gas Discharge Physics), Moscow: Intellekt, 2009.
- Raizer, Y.P., Milikh, G.M., and Shneider, M.N., Streamer- and leader-like processes in the upper atmosphere: Models of red sprites and blue jets, *J. Geophys. Res.*, 2010, vol. 115, A00E42. doi 10.1029/2009JA014645
- Stanley, M., Krehbiel, P., Brook, M., Moore, C., Rison, W., and Abrahams, B., High speed video of initial sprite development, *Geophys. Res. Lett.*, 1999, vol. 26, no. 20, pp. 3201–3204.
- Surkov, V.V. and Hayakawa, M., Underlying mechanisms of transient luminous events: A review, *Ann. Geophys.*, 2012, vol. 30, no. 8, pp. 1185–2012. doi 10.5194/angeo-30-1185-2012
- Surkov, V. and Hayakawa, M., *Ultra and Extremely Low Frequency Electromagnetic Fields*, Springer, 2014.

Translated by Yu. Safronov